[CANCER RESEARCH 64, 5570–5577, August 15, 2004]

Uterine Leiomyomata with t(10;17) Disrupt the Histone Acetyltransferase *MORF*

Steven D. P. Moore,[2,3] Steven R. Herrick,[1] Tan A. Ince,[1,3,4] Michael S. Kleinman,[1] Paola Dal Cin,[1,3] Cynthia C. Morton,[1,2,3] and Bradley J. Quade[1,3]

Departments of [1]Pathology, and [2]Obstetrics, Gynecology, and Reproductive Medicine, Brigham and Women's Hospital, Boston; [3]Harvard Medical School, Boston; and [4]Massachusetts Institute of Technology, Cambridge, Massachusetts

ABSTRACT

Benign uterine leiomyomata are the most common tumors in women of reproductive age. One recurring chromosomal aberration in uterine leiomyomata is rearrangement of 10q22. Chromosome 10 breakpoints were mapped by fluorescence *in situ* hybridization to intervals ranging from 8.9 to 72.1 kb within the third intron of *MORF* (monocytic leukemia zinc finger protein-related factor or *MYST4*) in four uterine leiomyomata tested. Additional Southern hybridization experiments confirmed that the breakpoint lies within the third intron and narrowed the interval to 2.1 kb in one uterine leiomyomata. *MORF* is a member of the MYST family of histone acetyltransferase and previously has been found rearranged in some types of acute myeloid leukemia (AML). This is the first instance in which disruption of a histone acetyltransferase has been reported in another tumor type. The breakpoints in uterine leiomyomata would fall in the NH_2-terminal portion of the protein between a conserved domain found in histones H1 and H5 and the PHD zinc fingers, the CH2CH zinc finger, or the CoA binding site, which is distinct from the breakpoints reported in AML. Mapping of the 17q21 breakpoint by fluorescence *in situ* hybridization within a specific region in three tumors revealed several positional candidates including *GCN5L2*, a gene with histone acetyltransferase activity similar to those fused to *MORF* in AML. Of note, two of three uterine leiomyomata were of the cellular subtype. Involvement of *MORF* in four uterine leiomyomata with chromosomal rearrangements involving 10q22 and 17q21 suggests a role for this histone acetyltransferase and altered chromatin regulation in uterine mesenchymal neoplasia.

INTRODUCTION

Benign uterine smooth muscle tumors, known as leiomyomata or fibroids, are the most common human neoplasm. These tumors occur in as many as 77% of women by their latter reproductive years and arise as multiple independent tumors (1–3). Approximately 20% of women experience symptoms including abnormal uterine bleeding, pelvic pain and pressure, infertility, and spontaneous abortion. Consequently, leiomyomata are the leading indication for hysterectomy, accounting for 2.1 procedures per 1000 women per year (4). In contrast, malignant tumors of uterine smooth muscle occur in 1% of hysterectomies for presumed "fibroids" between the ages of 40 and 60 years (5).

Approximately 40% of uterine leiomyomata have a simple chromosomal aberration (6). In contrast with malignant leiomyosarcoma, which typically have complex numerical and structural chromosomal aberrations, the karyotypic abnormalities found in leiomyomata are simple (7). Many of the abnormalities are recurrent, and at least six distinct subgroups have been defined: del(7)(q22q32), t(12;14)(q15; q24), rearrangements involving 3p, 6p, and 10q, as well as trisomy 12 (6, 8). The variety of rearrangements suggests that there is more than one molecular pathway leading to leiomyoma tumorigenesis. Rearrangements involving 6p21 and 12q15 are associated with aberrant expression of the nonhistone chromatin proteins *HMGA1* and *HMGA2* (9–11). The molecular mechanisms associated with the other rearrangements have yet to be defined.

In this report, we focus on the 10q22 breakpoint in uterine smooth muscle neoplasia. Ozisik *et al.* observed that 5% of chromosomally abnormal uterine leiomyomata had rearrangements of 10q22 (12). To date, 18 leiomyomata and 9 leiomyosarcomas have been reported with 10q22 breakpoints in the online Mitelman Database of Chromosome Aberrations in Cancer.[5] Most of these smooth muscle tumors had balanced translocations between chromosome 10 and a variety of partners including chromosomes 4, 6, or 12 in leiomyomata and chromosomes 7, 11, 17, or 18 in leiomyosarcomas. A less frequent rearrangement, del(10)(q22q24), is found in benign uterine smooth muscle tumors. Interestingly, t(10;17) has been reported as the sole cytogenetic abnormality in one leiomyosarcoma and as part of a complex karyotype in another leiomyosarcoma (7, 13). In addition, loss of 10q is very frequent in uterine leiomyosarcomas (14, 15).

We initially mapped the chromosome 10 breakpoint in a cellular leiomyomata with t(10;17) and found disruption of *MORF*, which is also known as monocytic leukemia zinc finger (*MOZ*) protein-related factor, *MOZ2*, *MYST4*, and *querkopf*. *MORF* is a member of the MYST family of histone actelyases (histone acetyltransferase), so named for the defining members *M*OZ, *Y*bf2/Sas3, *S*as2 (something about silencing 2), and *T*ip60 (HIV Tat-interacting protein of 60 kDa; Ref. 16). Histone acetyltransferases transfer an acetyl group from acetyl-CoA to the ϵ-amino group of lysine within the basic NH_2-termini of histones, which bind the acidic phosphates of DNA. MORF preferentially acetylates histones H3 and H4 as free monomers and H4 when assembled into nucleosomes (17). Acetylation of these tails reduces the affinity of nucleosomes for DNA, presumably allowing segments of DNA to become more accessible to other proteins such as transcription factors. The reversible nature of acetylation provides a potential regulatory mechanism.

MATERIALS AND METHODS

Tumor Samples. Uterine leiomyomata analyzed in this study were selected based on the presence of a chromosomal rearrangement involving 10q22. Their pathological and cytogenetic features are summarized in Table 1.

Tissues from tumors ST92–119 and ST02–391 were obtained from the Division of Women's and Perinatal Pathology in accordance with institutional policies concerning use of discarded human tissues. Tumor samples were disaggregated, cultured and karyotyped by GTG-banding according to established protocols (18). Histopathological diagnoses were determined by examination of hematoxylin and eosin stained tissue sections by two gynecological pathologists.

Frozen disaggregated cells were obtained from two tumors characterized by GTG-banded karyotypes by Dr. Avery Sandberg and colleagues at the Cancer Center of the Southwest Biomedical Research Institute (Scottsdale, AZ). These cells, now housed at Genzyme Corporation (Framingham, MA), were provided by Dr. Robert Pomponio (Genzyme Corporation). In this report, these tumors will be referred to by the designations SWBRI165 and SWBRI510. Tumor

Received 1/7/04; revised 6/11/04; accepted 6/11/04.

Grant support: American Cancer Society (RPG CNE-00–228-01; B. Quade), National Cancer Institute (CA78895; C. Morton), and a K08 award from the National Cancer Institute (CA 92013; T. Ince).

The costs of publication of this article were defrayed in part by the payment of page charges. This article must therefore be hereby marked *advertisement* in accordance with 18 U.S.C. Section 1734 solely to indicate this fact.

Requests for reprints: Bradley Quade, Department of Pathology, Brigham and Women's Hospital, 75 Francis Street, Boston, MA 02115. Phone: (617) 732-5475; Fax: (617) 738-6996; E-mail: bquade@partners.org.

[5] Internet address: http://cgap.nci.nih.gov/Chromosomes/Mitelman.

Table 1 *Summary of pathological and cytogenetic features for uterine leiomyomata with translocations involving 10q22*

Tumor	Histological subtype and tumor size	Karyotype*	FISH mapping method	Chromosome 17 breakpoint
ST02–391	Cellular, 12.5 cm	46,XX,t(10;17)(q22;q23)	Metaphase	RP11–60B4, CTD-2584C24, CTD-2509C
ST92–119	Cellular, 12 cm	46,XX,t(3;19)(q22;q13),t(10;17)(q24;q24)	Interphase	CTD-2509C6
SWBRI510	Not available for review	46,XX,t(6;10;17;15)(p21;q22;q21;q23–24),dic(13;21)(p13;p13)	Interphase	Not yet mapped
SWBRI165†	Typical, 8 cm	46,XX,t(4;10)(q21;q22),inv(6)(p15q13),t(6;10)(p21;q22), del(15)(q15q22) [14]	Interphase	RP11–60B4

* Karyotypes are based on interpretation of GTG-banded metaphase spreads, and breakpoint assignments may differ from assignments based on FISH breakpoint mapping.
† Tumor SWBRI165 has been reported previously as case 5 by Ozisik *et al.* (12).

SWBRI165 has been reported previously as case 5 by Ozisik *et al.* (12). Frozen cell suspensions were found to be nonviable; however, these archival cells were suitable for breakpoint mapping by interphase fluorescence *in situ* hybridization (FISH).

Cultured tumor cells from tumor ST02–391 were immortalized by the expression of human papilloma virus 16 E6/E7. To create amphotropic retroviruses, 10-cm dishes of 293T cells were cotransfected using Fugene (Roche Inc., Indianapolis, IN) with 8 μg of the amphotropic packaging plasmid pCL-10A1 (Imgenex) and the retroviral vector LXSN 16E6/E7 expressing HPV16 E6/E7 proteins (provided by D. A. Galloway, Fred Hutchinson Cancer Research Center, Seattle, WA; Ref. 19). Viral supernatants were harvested at 36 h and used to infect early passage leiomyoma cells with 8 μg/ml Polybrene. Typically, 50–70% of infection was achieved by use of this protocol as measured by parallel infections with a green fluorescent protein-expressing retrovirus. Infected cells were selected using G-418. Presence of the t(10;17) in the human papilloma virus E6/E7-transformed ST02–391 cell line was confirmed by both conventional cytogenetics and FISH with a genomic clone (RP11–155B22) spanning the chromosome 10 breakpoint in all of the cells examined. Both untransformed and transformed cells were used in breakpoint mapping with equivalent results.

Bacterial Artificial Chromosomes. Bacterial artificial chromosomes (BACs) were obtained from the RP11 library (BACPAC Resource Center at the Children's Hospital Oakland Research Institute, Oakland, CA). BACs from the CTD library were purchased from Invitrogen (Carlsbad, CA). End-sequenced and FISH-verified BACs (20) were selected for breakpoint mapping using the University of California Santa Cruz Biotechnology Genome Browser and Database (21).[6] DNA was isolated following a standard protocol consisting of alkaline lysis, neutralization, and ethanol precipitation.

Fluorescence *In Situ* Hybridization. Slides with metaphase chromosome spreads from ST02–391 were prepared using standard hypotonic lysis and fixation. For ST92–119, SWBRI165, and SWBRI510, interphase nuclei were prepared for FISH by modification of the standard hypotonic lysis and fixation using touch preparation slides from archival frozen disaggregated cells. BAC DNAs used for FISH probes were labeled with Spectrum Green or Spectrum Orange-dUTP using the Nick Translation Reagent kit from Vysis (Downers Grove, IL). A mixture of fluorochrome-labeled DNA and Cot-1 DNA (Vysis) was resuspended in 70% Hybrizol (Vysis) and applied to glass slides. Slides were processed in the HYBrite denaturation/hybridization system (Vysis) using standard parameters (80°C for 1 min, followed by 37°C overnight). Slides next were washed twice for 8 min in 2× SSC and 50% formamide at 42°C, followed by 2X SSC at 37°C for 8 min. 4′,6′-Diamidino-2-phenylindole hydrochloride was used as a counterstain. Results were acquired with a Zeiss Axioskop 2 epifluorescence microscope (Thornwood, NY) and Applied Imaging CytoVision cytogenetics workstation (Santa Clara, CA). A minimum of 30 and occasionally 50 interphase nuclei were scored unless otherwise noted.

Southern Hybridization. Genomic DNA was isolated from HPV E6/E7-transformed ST02–391 tumor cells and peripheral blood from an unrelated male control. Restriction enzymes (*e.g.*, *Eco*RI, *Mfe*I, and *Stu*I) and hybridization probes selected for analysis of the ST02–391 chromosome 10 breakpoint region and its flanking sequences were based on the July 2003 human reference sequence (UCSC version hg16, NCBI Build 34) produced by the International Human Genome Sequencing Consortium (21). Digested DNA (8 μg) was electrophoresed on 1% agarose gels, transferred on to Nylon-N + membranes (Amersham, Piscataway, NJ), and UV cross-linked as specified by the manufacturer (Stratagene, La Jolla, CA). Probes were prepared by PCR amplification of genomic DNA, followed by preparative agarose gel electrophoresis, excision of correctly sized bands, and gel extraction (Qiagen, Valencia, CA). The primers (and their respective sequences) for the 515-bp amplicon (designated B5) in which the breakpoint was ultimately detected were 391-B5L (5′-GAC AAG GGG TGA ATT TGA TGA-3′) and 391-B5R (5′-ACC TCT CAT TTT CCT GAT GAA G-3′). Amplified DNA was prepared for hybridization by labeling with [^{32}P]dCTP using the MegaPrime DNA labeling system (Amersham). Membranes were prehybridized with UltraHyb solution (Clontech, Palo Alto, CA) for 1 h at 42°C and hybridized overnight with 25-ng radiolabeled probe. Excess probe was removed by washing at room temperature with 2× SSC and 0.1% SDS for 30 min followed by 0.5× SSC and 0.1% SDS for 30 min at 60°C. Autoradiograms were exposed 5 days at −80°C with intensifying screens.

RESULTS

Mapping of the Chromosome 10 Breakpoint in Uterine Leiomyoma ST02–391. Cytogenetic analysis of a 12.5-cm cellular leiomyoma (ST02–391) revealed a simple karyotype in which the balanced t(10;17)(q22;q23) was the sole chromosomal abnormality (Table 1; Fig. 1*A*). In a series of experiments, BAC clones with known positions within the sequence of chromosome 10 were used to flank the chromosome 10 breakpoint by FISH. The breakpoint subsequently was mapped to RP11–155B22 (Fig. 1*B*). The location of the chromosome 10 breakpoint in ST02–391 was additionally refined by FISH mapping using BAC clones that overlap with RP11–155B22. Clones RP11–222G7 and CTD-2160F19 also hybridized to both derivative chromosomes 10 and 17, indicating that they shared the chromosome 10 breakpoint with RP11–155B22. In addition, clone RP11–90D9 hybridized to der(10), whereas clones CTD-2363A10, RP11–1076B24, and RP11–77G23 hybridized to der(17). The minimal region encompassing the chromosome 10 breakpoint in ST02–391 would be a 14.7-kb interval defined by the telomeric end of RP11–90D9 and the centromeric end of CTD-2363A10 (Fig. 2*A*, *top*). This minimal breakpoint region corresponds to the third intron of *MORF* and would result in the interruption of a translated polypeptide after the H15 domain and before the PHD zinc finger domain (Fig. 2*B*).

To confirm the chromosome 10 breakpoint mapping by FISH, Southern hybridization was performed using genomic DNA from ST02–391 tumor cells. In a series of experiments, eight probes were selected based on the absence of repetitive sequence and used to test for aberrant bands in more than one restriction digest. These probes covered the 14.7-kb breakpoint region defined by FISH, as well the flanking sequences. On the basis of our experience in FISH mapping of other chromosomal breakpoints, a breakpoint sometimes may be located as much as 5–10 kb beyond the region determined by FISH. Such inaccuracies in FISH breakpoint mapping are believed to occur because it is difficult to detect split FISH hybridization signals when the breakpoint is located close to the end of the human sequence in a BAC clone, particularly if the repeat content is high near the terminus (data not shown). Aberrant bands in the Southern hybridizations were only detected with one probe, which we designated B5 (Fig. 3*A*). The presence of aberrant bands in several restriction digests excludes the

[6] Internet address: http://genome.ucsc.edu/.

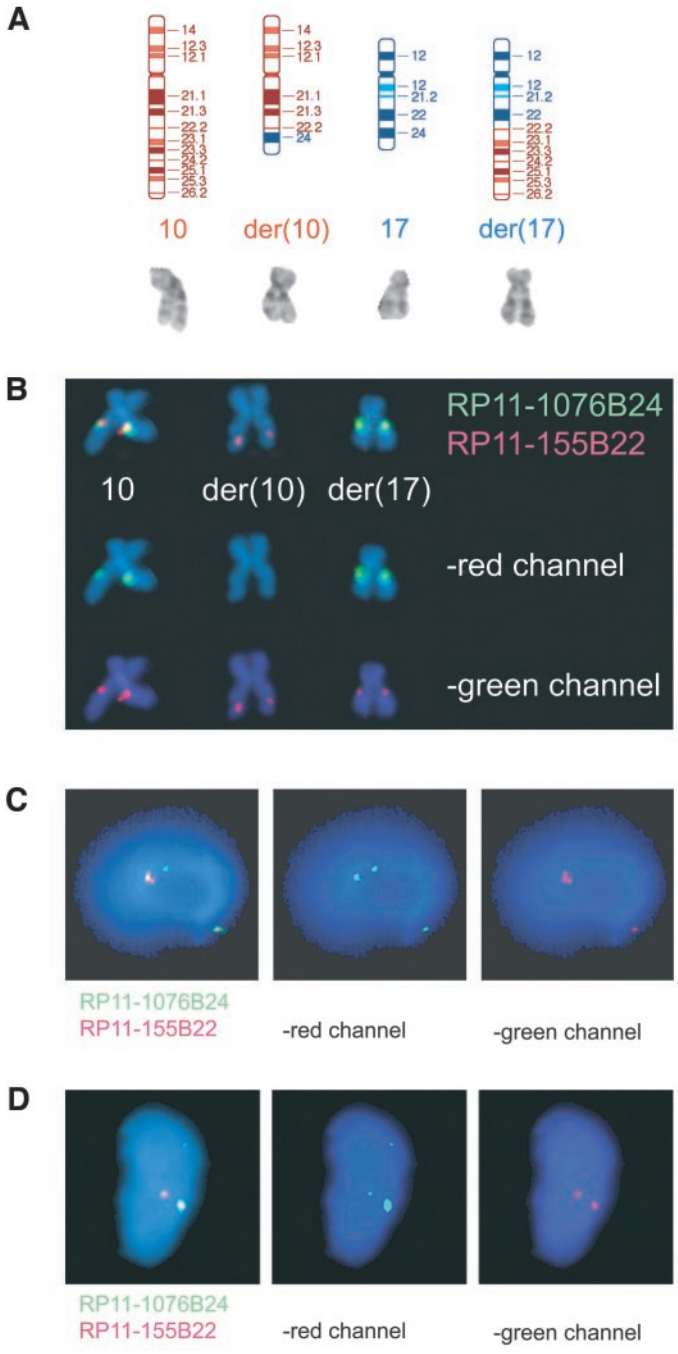

Fig. 1. Cytogenetic characterization of uterine leiomyoma (UL) with rearrangements of 10q22. *A*, partial GTG-banded karyotype and ideogram illustrating the t(10, 17)(q22;q23) in UL ST02–391. *B*, partial fluorescence *in situ* hybridization karyotype using probes on chromosome 10q22 and metaphase chromosomes from UL ST02–391 shows that the chromosome 10 breakpoint resides within bacterial artificial chromosome (BAC) RP11–155B22 (Spectrum Orange) and centromeric to bacterial artificial chromosome RP11–1076B24 (Spectrum Green). Image subtraction of the Spectrum Orange (*middle*) and Spectrum Green (*bottom*) signals from the composite image (*top*) is shown. *C* and *D*, interphase fluorescence *in situ* hybridization of tumors SWBRI510 (*C*) and SWBRI165 (*D*) localized the chromosome 10 breakpoint to RP11–1076B24 (Spectrum Green). The breakpoint in these tumors is telomeric to RP11–155B22 (Spectrum Orange). Image subtraction of the Spectrum Orange (*middle*) and Spectrum Green (*right*) signals from the composite image (*left*) was performed to separate overlapping signals.

possibility of a restriction length polymorphism and narrowed the breakpoint to within a 2,114-bp region (Fig. 3*B*). This region is located between *Mfe*I and *Eco*RI restriction sites at 75,965,747 and 75,967,861 bp, respectively, in the human chromosome 10 sequence (UCSC version hg 16). Furthermore, this region is located 10.2 kb from the nearest boundary of the FISH-defined breakpoint region, as defined by the terminus of BAC RP11–90D9. More importantly, the Southern-defined breakpoint region is located 17.9 kb from the third (and first coding) exon. Consequently, Southern hybridization analysis confirms that *MORF* is disrupted in the third intron in ST02–391.

***MORF* Is Disrupted in Other Uterine Leiomyoma with Rearrangements of Chromosomes 10 and 17.** Three other uterine leiomyomata with rearrangements of 10q22 were identified (Table 1). Interestingly, all of these uterine leiomyomata also had breakpoints involving 17q. The chromosome 10 breakpoint in archival samples of these tumors was assessed by interphase FISH with BAC clones in the *MORF* locus.

The first archival case evaluated, uterine leiomyoma ST92–119, had a balanced translocation t(10;17)(q24;q24). The band assignments determined by GTG-banding for the chromosome 10 and 17 breakpoints were similar to those of ST02–391, suggesting that the translocations in the two tumors could be the same. Two-color interphase FISH of ST92–119 with RP11–155B22 labeled in Spectrum Orange and RP11–77G23 labeled in Spectrum Green showed distinct red, green, and yellow or paired signals in all 30 of the nuclei analyzed (data not shown). Similar results were found with RP11–1076B24. Separation of nearby clones is indicative of a chromosomal rearrangement between the clones. In another experiment, the overlapping clones CTD-2160F19 and CTD-2363A10 hybridized to different derivative chromosomes in five nuclei analyzed (data not shown). This result suggested that the breakpoint in this tumor was in or near the segment shared by the overlapping clones. In a follow-up experiment, three signals for CTD-2363A10 were detected in 13 of 34 interphase nuclei examined; two signals were observed in the remainder. These results, summarized in the middle portion of Fig. 2*A*, are consistent with a minimal breakpoint region of $<$8.9 kb. This is a conservative estimate based on the interval between CTD-2160F19 and RP11–1076B24. A less conservative estimate would use the telomeric terminus of RP11–155B22, which ends 4 bp before RP11–1076B24. In either case, this region falls in the third intron of *MORF*. Furthermore, the minimal breakpoint region in ST92–119 is adjacent to the breakpoint region in ST02–391 and would disrupt the *MORF* polypeptide at the same point (Fig. 2*B*).

The next tumor analyzed, SWBRI510, had a more complex karyotype that involved breakpoints in 10q22, 17q21, 6p21, and 15q23–24 (Table 1). Interphase FISH with RP11–155B22 showed two signals in all of the nuclei. FISH with RP11–1076B23 or RP11–77G23 labeled with Spectrum Green showed three green signals in 23 and 26 of 30 nuclei, respectively. As illustrated in Fig. 1*C*, two of the three green signals colocalized with the RP11–155B22 signals labeled with Spectrum Orange, whereas the third green signal was separate. Four nuclei had just two green signals, both of which colocalized with the red signals. Such a result usually suggests that the tumor is cytogenetically mosaic or commingled with normal cells. Alternatively, diminished hybridization efficiency could have occurred during prolonged storage. In a final experiment, one set of signals for RP11–155B22 and RP11–455I15 were spatially separated in all 30 of the nuclei (data not shown). This finding indicates that the chromosome 10 breakpoint occurred in the *MORF* locus telomeric to the breakpoints found in ST02–391 and ST92–119. The minimal overlapping region based on this data would be 72.1 kb (Fig. 2*A*, *bottom*). This breakpoint could be positioned anywhere from the third to the twelfth intron of *MORF*. Most of this interval, however, is composed of the third intron, raising the possibility that the breakpoint in this tumor could result in a disruption equivalent to ST02–391 and ST92–119 (Fig. 2*B*). If the breakpoint were to be at the telomeric boundary, the disruption in the polypeptide at most would be NH_2-terminal to the acetyl-CoA binding site in the histone acetyltransferase domain.

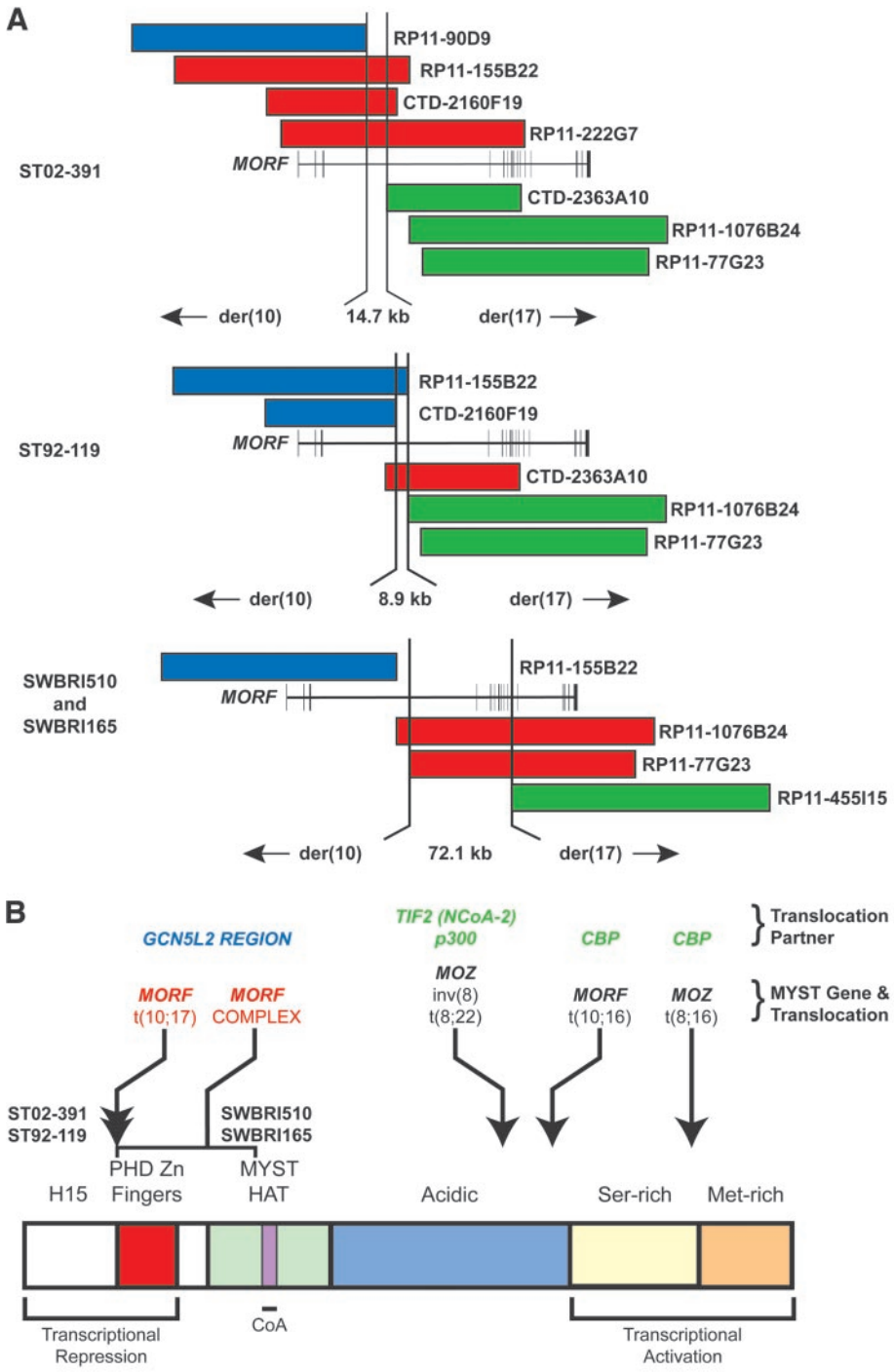

Fig. 2. Mapping of the chromosome 10 breakpoint within *MORF*. Fluorescence *in situ* hybridization mapping results for tumors ST02–391 (*top*), ST92–119 (*middle*), SWBRI510 and SWBRI165 (*bottom*) are shown in *A*. Bacterial artificial chromosome clone and gene alignment are based on the University of California Santa Cruz Biotechnology Genome Browser (version hg16, July 2003 assembly). Bacterial artificial chromosome clones hybridizing to der (10) and der (17) are shown in *blue* and *green*, respectively. Those clones hybridizing to both derivatives are shown in *red*. The minimal breakpoint regions (14.7 kb in ST02–391, 8.9 kb in ST92–119, and 72.1 kb in SWBRI510 and SWBRI165) are indicated by the *vertical lines*. The *vertical lines* in the *MORF* track denote exons. Mapped breakpoints in uterine leiomyomata (*red*) and acute myeloid leukemia (black) are shown relative to the functional domains of *MORF* and *MOZ* in *B* (27, 28, 44–50). The respective translocations and translocation partners also are illustrated in *black* and *green lettering* for acute myeloid leukemia and in *red* and *blue lettering* for leiomyomata, respectively. The *double arrowhead* or *horizontal bracket* and leiomyomata case numbers denote the predicted point of disruption.

The final tumor analyzed, SWBRI165, had a complex karyotype that was reported to include two balanced translocations involving 10q22, one with 4q21 and the other with 6p21 (Table 1). Interphase FISH with RP11–155B22 detected only two hybridization signals in all 30 of the nuclei. Experiments with RP11–1076B24 and RP11–77G23 detected three hybridization signals in 28 of 50 and 9 of 30 nuclei, respectively. Fig. 1*D* shows a pattern of hybridization in SWBRI165, which is the same pattern as that observed for SWBRI510. In another experiment, one of the signals for both RP11–155B22 and RP11–455I15 were spatially separated in 30 interphase nuclei examined, indicating that the breakpoint in *MORF* was between the two clones in SWBRI165. These results are identical to those obtained for SWBRI510 (Fig. 2*A*, *bottom*). Furthermore, it suggests that only one of the two chromosomes with rearrangements of 10q22 involved *MORF*. Finally, these data raise the possibility that SWBRI165 and SWBRI510 may share a common breakpoint that is distinct from those in ST02–391 and ST92–119 but that nevertheless results in mRNA products disrupted at the same point in all four of the tumors (Fig. 2*B*).

Mapping the Chromosome 17 Breakpoint in Uterine Leiomyomata ST02–391. In three of the four uterine leiomyomata, the10q22 rearrangement also involves a cytogenetically visible locus on 17q. Although the band assignment of the chromosome 17 breakpoint ranged from q21 to q24, it was reasonable to hypothesize that breakpoints in all three of the tumors might have been the same. Variability in breakpoint band assignment is not unprecedented and might be

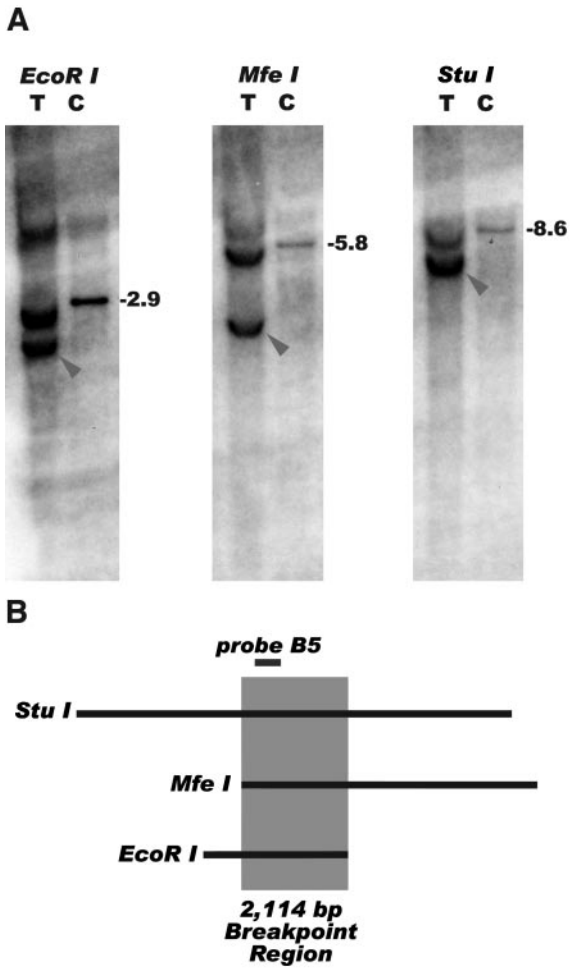

Fig. 3. Mapping of the chromosome 10 breakpoint in leiomyoma ST02–391 by Southern blot analysis. *A*, genomic DNA from ST02–391 tumor cells (*T*) and an unrelated control (*C*) was digested with *Eco*RI, *Mfe*I, and *Stu*I and the corresponding Southern blot was probed with PCR amplicon B5. The sizes of expected fragments, based on human genomic sequence (University of California Santa Cruz version hg 16), are shown to the *right* of each control lane. Aberrant bands in the tumor cell lanes are indicated by *arrowheads*. *B*, genomic map of the restriction fragments (denoted by *long horizontal lines*) expected to be detected by probe B5 (*short horizontal line*). As aberrant bands were detected by all three enzymes, the breakpoint must be located in the overlapping 2,114 bp (denoted by the *shaded rectangle*). The boundaries of this region are located 17.9 kb downstream (telomeric) of the third (and first coding) exon and 10.2 kb upstream (centromeric) of bacterial artificial chromosome clone RP11–90D9 terminus.

attributable to biological (*e.g.*, chromosome condensation between tumors or individuals), technical, or interpretive differences. To test this hypothesis, the chromosome 17 breakpoint first was mapped in ST02–391 using the same approach as that for mapping the chromosome 10 breakpoint. Initial experiments did not flank the breakpoint and showed that BAC clones in 17q24 hybridized telomeric to the breakpoint. Subsequent experiments walking centromerically were performed until the breakpoint was flanked using clones mapped to 17q21. The first clone hybridizing to both the der(10) and der(17) was RP11–60B4. Fine mapping with clones overlapping RP11–60B4 showed that clones CTD-2584C24 and CTD-2509C6 also contained the chromosome 17 breakpoint. In addition, CTD-2346B3 (*blue*) was centromeric to the breakpoint, and CTD-2507A6 (*green*) was telomeric to the breakpoint (Fig. 4*A*). The minimal breakpoint region defined by these results was 32.8 kb. Three genes are partially or entirely mapped within this interval, *GCN5L2*, *HspB9*, and *RAB5C*.

To determine whether the same breakpoint was present in the other tumors, interphase FISH was performed with selected chromosome 17 probes. In ST92–119, CTD-2509C6 was detected in three sites of hybridization in 18 of 35 nuclei examined (Fig. 4*B*). FISH analysis of the same tumor with RP11–60B4 revealed evidence of the rearrangement in only 4 of 31 nuclei examined. In these 4 nuclei, RP11–60B4 colocalized with a *MORF*-specific probe (RP11–155B22; data not shown). It is possible that the disruption of RP11–60B4 is difficult to detect because it is eccentrically located within that clone. Localization of the 17q breakpoint within two overlapping clones in two different tumors suggests that the region, and perhaps a specific gene, is fused preferentially to the *MORF* locus by the rearrangement.

Interphase FISH analysis with either RP11–60B4 or CTD-2509C6 did not detect evidence of a breakpoint in SWBRI510, a tumor with a four-way translocation involving chromosomes 6, 10, 15, and 17. Interesting, evidence of a cryptic chromosome 17 rearrangement was found in SWBRI165, the tumor in which rearrangement of chromosome 17 had not been appreciated by GTG-banding. Three RP11–60B4 hybridization signals were found in 27 of 50 nuclei examined. In an experiment with two-color FISH, the chromosome 17 probe RP11–60B4 colocalized with the chromosome 10 probe RP11–1076B24 twice in each nuclei, presumably once for each derivative chromosome of the cryptic rearrangement (Fig. 4*C*). In summary, three of the four uterine leiomyomata with *MORF* rearrangements also involved a particular region on 17q21.

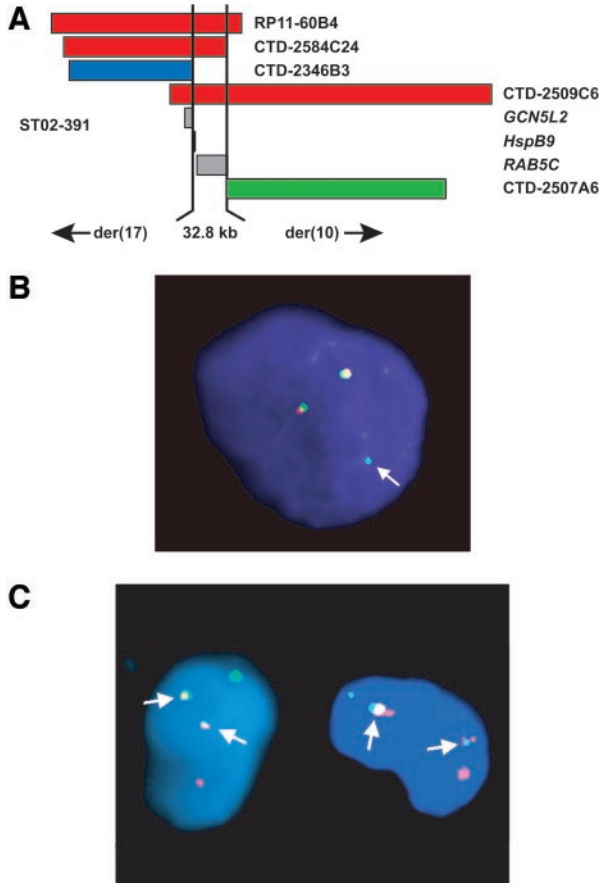

Fig. 4. Mapping of the chromosome 17 breakpoint. *A*, schematic of fluorescence *in situ* hybridization (FISH) breakpoint mapping in UL ST02–391. Bacterial artificial chromosome clones hybridizing to either der (10) or der (17) are shown in *blue* (CTD-2346B3) and *green* (CTD-2507A6), respectively. Those clones hybridizing to both derivatives are shown in *red*. The minimal breakpoint region (32.8 kb) is indicated by the *vertical lines*. The *gray boxes* indicate the three genes (*GCN5L2*, *HspB9*, and *RAB5C*) that overlap with the minimal breakpoint region. *B*, interphase FISH of uterine leiomyoma ST92–119 with two overlapping clones, RP11–60B4 (Spectrum Orange) and CTD-2509C6 (Spectrum Green), on 17q21. The *arrow* indicates a green signal that does not colocalize with a red signal. *C*, interphase FISH of uterine leiomyoma SWBRI165 with a chromosome 10 probe (RP11–1076B24) labeled with Spectrum Green and a chromosome 17 probe (RP11–60B4) labeled with Spectrum Orange. Two representative nuclei are illustrated. Colocalization of the two probes is indicated by *arrows*.

Correlation with Histological Phenotype. Features that have been used in the determination of malignancy in uterine smooth muscle neoplasms include geographic tumor necrosis, nuclear and cytoplasmic atypia, proliferative activity, hypercellularity, intravascular growth, and metastasis (22, 23). Benign leiomyoma variants in the uterus are defined by each of these features. The molecular factors contributing to the phenotypes of these benign variants have yet to be fully elucidated. To determine whether *MORF* disruption correlated with a particular histological phenotype, we examined tissue sections from the two available tumors (ST02–391 and ST92–119). Interestingly, the original gynecological pathologists had classified both tumors as cellular leiomyomata. Upon our review, both tumors had distinct hypercellularity sufficient to confirm the original diagnosis. SWBRI165 was reported to have a typical histology (12).

DISCUSSION

Four uterine leiomyomata were found to have disruptions in *MORF* on chromosome 10 band q22. The recurrence of the same breakpoint in tumors from different individuals strongly suggests that this rearrangement does indeed represent a cytogenetically distinct subgroup of uterine leiomyomata. This notion additionally is reinforced by the observation that the translocation partner was located in a specific region of 17q21 in three of the four tumors. The chromosomal aberrations also involved 17q21 in the fourth tumor, but the breakpoint was not located in same specific interval defined by two overlapping BAC clones. This group also may be defined by a common phenotype. Specifically, two of three tumors available for pathological review were of a particular histological subtype, namely the cellular variant. Interestingly, another tumor (case 3) in a series of nine uterine leiomyomata with 10q22 rearrangements was classified as a cellular uterine leiomyomata (12). Cellular leiomyoma, such as those in this report, are of concern because they morphologically mimic malignant endometrial stromal sarcomas (24). In addition, an uterine leiomyosarcoma in which the sole abnormality was t(10;17) might have been misclassified and may actually belong with this group of histologically unusual uterine leiomyomata. Finally, the involvement of *MORF*, the third gene to be identified in uterine leiomyomata by positional methods, suggests a mechanistic role for this histone acetyltransferase in this distinct subgroup.

The chromosome 10 breakpoint localized to the third intron of *MORF* in at least two and possibly all four of the tumors (Fig. 2). Like other MYST family members, *MORF* contains a MYST homology domain composed of an acetyl-CoA binding site and a C2HC zinc finger motif. The 1781 residue product of *MORF* is most related (60% identity and 66% similarity) to the 2004 residue product of *MOZ*, also known as *MOZ1*, monocytic leukemia zinc ring finger protein, *MYST3*, or *ZNF220* (17). Both contain two additional C4HC3 PHD (the so-called plant homeo domain) zinc finger domains, which are implicated to be protein-protein or protein-phospholipid interactions playing a role in eukaryotic gene regulation (25). In addition, both *MORF* and *MOZ* have a domain (H15) that is homologous to the linker (*i.e.*, noncore) histones H1 and H5, proteins that are believed to stabilize higher orders of chromatin folding. The translocation in leiomyomata apparently disrupts MORF in the NH_2-terminal portion of the protein between the H15 domain and the PHD zinc fingers, the C2HC zinc finger, or the acetyl-CoA binding site of the histone acetyltransferase domain.

Several cancers have been associated with rearrangement of MYST histone acetyltransferases. For example, disruption of *MOZ* at 8p11 has been found in M4/M5 subtypes of acute myeloid leukemia (AML) with the recurrent translocation t(8;16)(p11;p13). This translocation fuses the H15, PHD zinc finger, and histone acetyltransferase domains in-frame to a largely intact cyclic AMP response element binding protein (26). *MOZ* also is fused in other cases of AML to *p300* with the translocation t(8;22)(p11;q13) and to *TIF2* (*NCOA2* or nuclear receptor coactivator 2) with the inversion inv(8)(p11q13) (27, 28). More recently, Panagopoulos *et al.* (29) showed that a translocation t(10;16)(q22;p13) in a case of childhood AML, M5a subtype, resulted in an in-frame fusion between *MORF* and cyclic AMP response element binding protein. The fusion transcript contained the zinc finger domains, two nuclear translocation signals, the histone acetyltransferase domain, and a portion of the central acidic domain of *MORF* joined to cyclic AMP response element binding protein after codon 29 of the latter. Consequently, the *MORF*-cyclic AMP response element binding protein fusion transcript would also contain the RARA-binding domain, the cyclic AMP response element binding protein-binding domain, the three Cys/His-rich regions, the bromodomain, the histone acetyltransferase domain, and the Glu-rich domain of cyclic AMP response element binding protein. This report, however, is the first time in which a histone acetyltransferase has been found to be rearranged in uterine leiomyomata. In comparison to the reported hematopoietic malignancies, the disruption of *MORF* in uterine leiomyomata appears to be more 5′ in the locus.

The mechanisms by which *MOZ* and *MORF* fusions appear to play a critical role in oncogenesis have yet to be elucidated fully. It has been hypothesized that their fusion transcripts have misdirected histone acetyltransferase activity, which presumably allows altered transcriptional regulation. A second explanation is based on the observation that transcriptional repression and activation domains are found in the NH_2-terminal and COOH-terminal regions of these proteins (Fig. 2; Ref. 17). Thus, a chromosomal rearrangement may separate these domains or join them to another gene. With regard to *MOZ*, these domains interact with the *RUNX1* (runt-related transcription factor 1 or *AML1*)-*CBFβ* complex and stimulate hematopoietic cell-specific transcription (30). The *MOZ*-cyclic AMP response element binding protein fusion, however, inhibits *RUNX1*-mediated transcription. *MOZ* and *MORF* also interact with the related protein, *RUNX2* (runt related transcription factor 2 or *AML3*). Furthermore, the COOH-terminal Ser and Met-rich domains of *MORF* potentiate *RUNX2*-dependent transcription (31). It is interesting to note that the *RUNX1* transcript is up-regulated 3.7-fold in leiomyoma and 18.2-fold in leiomyosarcoma compared with myometrium (32). The increase in *RUNX1* expression is one of the largest changes in a smooth muscle tumor transcriptional profile more frequently characterized by down-regulation. Thus, *MORF* and *MOZ* may contribute to oncogenesis either by acetylation of either histones or transcription factors, or by interacting with transcription complexes via the NH_2-terminal and COOH-terminal domains.

More recently, Deguchi *et al.* (33) have proposed a third mechanism by which *MOZ* and *MORF* fusions might cause AML. In their studies, they tested various deletion mutants of *MOZ-TIF2* for their capacity to produce leukemia in a murine bone marrow transplant model. Interestingly, they found that the PHD zinc fingers were dispensable, but the histone acetyltransferase domain was required. In follow-up studies in which either the C2CH zinc finger or the acetyl-CoA binding site was altered by inactivating point mutations, Deguchi *et al.* (33) showed that *MOZ* histone acetyltransferase activity *per se* is not required for leukemogenesis. They hypothesized that the key contribution of *MOZ* to the fusion gene is the nucleosome recognition domain provided by the unusual C2CH zinc finger domain next to the catalytic acetyl-CoA binding site (33, 34). If the same mechanism were to be applied to uterine leiomyomata, then one might expect that a fusion transcript derived from der(17) (*i.e.*, the one with the portion telomeric to the chromosome 10 breakpoint) would be pathogenetic. The reciprocal transcript, which contains potentially only the H15

domain, would not be predicted to contribute to uterine leiomyomata pathogenesis in this third mechanism.

In this third mechanism, TIF2 contributes to leukemogenesis by recruiting cyclic AMP response element binding protein (and its histone acetyltransferase activity) to unspecified nucleosomal targets (33). It is possible that the translocation partner on chromosome 17 makes a similar contribution in the pathobiology of uterine leiomyomata. Molecular cytogenetic mapping of the chromosome 17 breakpoint showed that the breakpoint was within a 32.8-kb interval within BAC RP11–60B4 in tumor ST02–391. In addition, the chromosome 17 breakpoint mapped within this region in two other tumors. Interestingly, one of these tumors, SWBRI165, was not reported as having a rearrangement involving chromosome 17 by GTG-banded karyotype analysis. This observation raised the possibility of a cryptic aberration. The chromosome 17 breakpoint may be heterogeneous, as evidenced by the inability to detect rearrangement in this region for tumor SWBRI510. This particular tumor has a complex four-way rearrangement. Localization of the chromosome 17 breakpoint to the 32.8-kb interval implicated three genes as potential candidates as potential *MORF* fusion partners in uterine leiomyomata with t(10;17). These three genes include the second human homologue of a yeast transcription factor and histone acetyltransferase (*GCN5L2*), a small heat shock protein gene (*HspB9*), and a *ras* oncogene family member (*RAB5C*). On the basis of the similar biology (*i.e.*, histone acetyltransferase activity and the parallel to translocations involving *MORF* and *MOZ* in AML), *GCN5L2* could be deemed the most attractive of the three positional candidates.

GCN5L2 is a homologue of a yeast histone acetyltransferase, sharing 43% identity. The histone acetyltransferase domain of human *GCN5L2* can complement yeast *gcn5* null mutants and acetylates histone cores (35). Mammalian *GCN5L2* and *PCAF* (*p*300/cyclic AMP response element binding protein associated factor/general control nonrepressible 5) share a homologous NH_2-terminal domain important for recognition and acetylation of nucleosomes (36). Like PCAF, GCN5L2 interacts with p300 and cyclic AMP response element binding protein (36). Therefore, it is possible that GCN5L2 either substitutes for p300 and cyclic AMP response element binding protein in smooth muscle tumor-associated fusions or the fusion product recruits PCAF or cyclic AMP response element binding protein proteins, similar to the cyclic AMP response element binding protein interaction domain of *TIF2* in *MOZ-TIF2* fusion (33).

In addition to *MORF* and *GCN5L2*, other chromosomal rearrangements in uterine leiomyomata involve chromatin-associated genes. Specifically, rearrangements of 12q15 involve the *HMGA2* locus (37, 38). HMGA2 (formerly HMGI-C), originally named for its high mobility during electrophoresis of nonhistone chromosomal proteins, is a DNA architectural protein (39, 40). The DNA binding activity of HMGA2 is mediated by three AT hook domains encoded by the first three exons (41). It differs from its closely related family member HMGA1 [formerly *HMGI(Y)*] in the acidic COOH-terminal domain. *HMGA1*, which is located at 6p21, also is rearranged in some uterine leiomyomata. In addition, *HMGA1* participates in the assembly of the enhanceosome, a higher order chromatin enhancer complex, in response to viral infection (42). Enhanceosomal activation of interferon β transcription is regulated by HMGA1 acetylation (43). Specifically, acetylation of HMGA1 at Lys65 by p300/cyclic AMP response element binding protein destabilizes the enhanceosome. Acetylation at Lys71 by PCAF/GCN5, however, blocks acetylation by p300/cyclic AMP response element binding protein and stabilizes the enhanceosome. Consequently, HMGA1 and HMGA2 might be regarded as potential targets of the MORF fusion product in uterine leiomyomata.

The conjunction of observations that two different types of chromatin proteins (HMG proteins and histone acetyltransferases) are involved in smooth muscle tumors suggests that chromatin regulation plays an important role in their tumorigenesis. Chromatin alterations of by DNA bending (HMG proteins) or nucleosome dissociation (histone acetyltransferases) are potential mechanisms. Another potential mechanism is acetylation of HMG proteins (or other transcriptional factors) by *MORF* fusions, which consequently might change the pattern of enhanceosome-mediated transcription. The resulting transcriptional aberrations may in turn stimulate tumor cell growth and account for the cellular phenotype of uterine leiomyoma with t(10;17).

REFERENCES

1. Cramer SF, Patel A. The frequency of uterine leiomyomas. Am J Clin Pathol 1990;94:435–8.
2. Linder D, Gartler SM. Glucose-6-phosphate dehydrogenase mosaicism: utilization as a cell marker in the study of leiomyomas. Science 1965;150:67–9.
3. Townsend DE, Sparkes RS, Baluda MC, McClelland G. Unicellular histogenesis of uterine leiomyomas as determined by electrophoresis by glucose-6-phosphate dehydrogenase. Am J Obstet Gynecol 1970;107:1168–73.
4. Keshavarz H, Hillis SD, Kieke BA, Marchbanks PA. Hysterectomy Surveillance —United States, 1994–1999. MMWR 2002;51:1–8.
5. Leibsohn S, d'Ablaing G, Mishell DR Jr, Schlaerth JB. Leiomyosarcoma in a series of hysterectomies performed for presumed uterine leiomyomas. Am J Obstet Gynecol 1990;162:968–74.
6. Ligon AH, Morton CC. Genetics of uterine leiomyomata. Genes Chromosomes Cancer 2000;28:235–45.
7. Fletcher JA, Morton CC, Pavelka K, Lage JM. Chromosome aberrations in uterine smooth muscle tumors: potential diagnostic relevance of cytogenetic instability. Cancer Res 1990;50:4092–7.
8. Ligon AH, Morton CC. Leiomyomata: heritability and cytogenetic studies. Hum Reprod Update 2001;7:8–14.
9. Kazmierczak B, Dal Cin P, Wanschura S, et al. HMGIY is the target of 6p21.3 rearrangements in various benign mesenchymal tumors. Genes Chromosomes Cancer 1998;23:279–85.
10. Sornberger KS, Weremowicz S, Williams AJ, et al. Expression of HMGIY in three uterine leiomyomata with complex rearrangements of chromosome 6. Cancer Genet Cytogenet 1999;114:9–16.
11. Quade BJ, Weremowicz S, Neskey DM, et al. Fusion transcripts involving HMGA2 are not a common molecular mechanism in uterine leiomyomata with rearrangements in 12q15. Cancer Res 2003;63:1351–8.
12. Ozisik YY, Meloni AM, Surti U, Sandberg AA. Involvement of 10q22 in leiomyoma. Cancer Genet Cytogenet 1993;69:132–5.
13. Dal Cin P, Boghosian L, Crickard K, Sandberg AA. t(10;17) as the sole chromosome change in a uterine leiomyosarcoma. Cancer Genet Cytogenet 1988;32:263–6.
14. Quade BJ, Pinto AP, Howard DR, Peters WA III, Crum CP. Frequent loss of heterozygosity for chromosome 10 in uterine leiomyosarcoma in contrast to leiomyoma. Am J Pathol 1999;154:945–50.
15. Hu J, Khanna V, Jones M, Surti U. Genomic alterations in uterine leiomyosarcomas: potential markers for clinical diagnosis and prognosis. Genes Chromosomes Cancer 2001;31:117–24.
16. Sterner DE, Berger SL. Acetylation of histones and transcription-related factors. Microbiol Mol Biol Rev 2000;64:435–59.
17. Champagne N, Bertos NR, Pelletier N, et al. Identification of a human histone acetyltransferase related to monocytic leukemia zinc finger protein. J Biol Chem 1999;274:28528–36.
18. Rein MS, Friedman AJ, Barbieri RL, Pavelka K, Fletcher JA, Morton CC. Cytogenetic abnormalities in uterine leiomyomata. Obstet Gynecol 1991;77:923–6.
19. Foster SA, Galloway DA. Human papillomavirus type 16 E7 alleviates a proliferation block in early passage human mammary epithelial cells. Oncogene 1996;12:1773–9.
20. Cheung VG, Nowak N, Jang W, et al. Integration of cytogenetic landmarks into the draft sequence of the human genome. Nature 2001;409:953–8.
21. Karolchik D, Baertsch R, Diekhans M, et al. The UCSC Genome Browser Database. Nucleic Acids Res 2003;31:51–4.
22. Bell SW, Kempson RL, Hendrickson MR. Problematic uterine smooth muscle neoplasms. A clinicopathologic study of 213 cases. Am J Surg Pathol 1994;18:535–58.
23. Quade BJ. Pathology, cytogenetics and molecular biology of uterine leiomyomas and other smooth muscle lesions. Curr Opin Obstet Gynecol 1995;7:35–42.
24. Nucci MR, O'Connell JT, Huettner PC, Cviko A, Sun D, Quade BJ. h-Caldesmon expression effectively distinguishes endometrial stromal tumors from uterine smooth muscle tumors. Am J Surg Pathol 2001;25:455–63.
25. Gozani O, Karuman P, Jones DR, et al. The PHD finger of the chromatin-associated protein ING2 functions as a nuclear phosphoinositide receptor. Cell 2003;114:99–111.
26. Borrow J, Stanton VP, Jr., Andresen JM, et al. The translocation t(8;16)(p11;p13) of acute myeloid leukaemia fuses a putative acetyltransferase to the CREB-binding protein. Nat Genet 1996;14:33–41.
27. Kitabayashi I, Aikawa Y, Yokoyama A, et al. Fusion of MOZ and p300 histone acetyltransferases in acute monocytic leukemia with a t(8;22)(p11;q13) chromosome translocation. Leukemia 2001;15:89–94.

28. Carapeti M, Aguiar RC, Watmore AE, Goldman JM, Cross NC. Consistent fusion of MOZ and TIF2 in AML with inv(8)(p11q13). Cancer Genet Cytogenet 1999;113: 70–2.
29. Panagopoulos I, Fioretos T, Isaksson M, et al. Fusion of the MORF and CBP genes in acute myeloid leukemia with the t(10;16)(q22;p13). Hum Mol Genet 2001;10: 395–404.
30. Kitabayashi I, Aikawa Y, Nguyen LA, Yokoyama A, Ohki M. Activation of AML1-mediated transcription by MOZ and inhibition by the MOZ-CBP fusion protein. EMBO J 2001;20:7184–96.
31. Champagne N, Pelletier N, Yang XJ. The monocytic leukemia zinc finger protein MOZ is a histone acetyltransferase. Oncogene 2001;20:404–9.
32. Quade BJ, Wang TY, Sornberger K, Dal Cin P, Mutter GL, Morton CC. Molecular pathogenesis of uterine smooth muscle tumors from transcriptional profiling. Genes Chromosomes Cancer 2004;40:97–108.
33. Deguchi K, Ayton PM, Carapeti M, et al. MOZ-TIF2-induced acute myeloid leukemia requires the MOZ nucleosome binding motif and TIF2-mediated recruitment of CBP. Cancer Cell 2003;3:259–71.
34. Akhtar A, Becker PB. The histone H4 acetyltransferase MOF uses a C2HC zinc finger for substrate recognition. EMBO Rep 2001;2:113–8.
35. Wang L, Mizzen C, Ying C, et al. Histone acetyltransferase activity is conserved between yeast and human GCN5 and is required for complementation of growth and transcriptional activation. Mol Cell Biol 1997;17:519–27.
36. Xu W, Edmondson DG, Roth SY. Mammalian GCN5 and P/CAF acetyltransferases have homologous amino-terminal domains important for recognition of nucleosomal substrates. Mol Cell Biol 1998;18:5659–69.
37. Ashar HR, Fejzo MS, Tkachenko A, et al. Disruption of the architectural factor *HMGI-C*: DNA-binding AT hook motifs fused in lipomas to distinct transcriptional regulatory domains. Cell 1995;82:57–65.
38. Schoenmakers EFPM, Wanschura S, Mols R, Bullerdiek J, Van Den Berghe H, Van de Ven WJM. Recurrent rearrangements in the high mobility group protein gene, HMGI-C, in benign mesenchymal tumours Nat Genet 1995;10:436–44.
39. Reeves R, Beckerbauer L. HMGI/Y proteins: flexible regulators of transcription and chromatin structure. Biochim Biophys Acta 2001;1519:13–29.
40. Bustin M. Revised nomenclature for high mobility group (HMG) chromosomal proteins. Trends Biochem Sci 2001;26:152–3.
41. Reeves R. Structure and function of the HMGI(Y) family of architectural transcription factors. Environ Health Perspect. 2000;108 Suppl 5:803–9.
42. Thanos D, Maniatis T. Virus induction of human IFN beta gene expression requires the assembly of an enhanceosome. Cell 1995;83:1091–100.
43. Munshi N, Merika M, Yie J, Senger K, Chen G, Thanos D. Acetylation of HMG I(Y) by CBP turns off IFN beta expression by disrupting the enhanceosome. Mol Cell 1998;2:457–67.
44. Carapeti M, Aguiar RC, Goldman JM, Cross NC. A novel fusion between MOZ and the nuclear receptor coactivator TIF2 in acute myeloid leukemia. Blood 1998;91: 3127–33.
45. Chaffanet M, Gressin L, Preudhomme C, Soenen-Cornu V, Birnbaum D, Pebusque MJ. MOZ is fused to p300 in an acute monocytic leukemia with t(8;22). Genes Chromosomes Cancer 2000;28:138–44.
46. Chaffanet M, Mozziconacci MJ, Fernandez F, et al. A case of inv(8)(p11q24) associated with acute myeloid leukemia involves the MOZ and CBP genes in a masked t(8;16). Genes Chromosomes Cancer 1999;26:161–5.
47. Liang J, Prouty L, Williams BJ, Dayton MA, Blanchard KL. Acute mixed lineage leukemia with an inv(8)(p11q13) resulting in fusion of the genes for MOZ and TIF2. Blood 1998;92:2118–22.
48. Panagopoulos I, Isaksson M, Lindvall C, Hagemeijer A, Mitelman F, Johansson B. Genomic characterization of MOZ/CBP and CBP/MOZ chimeras in acute myeloid leukemia suggests the involvement of a damage-repair mechanism in the origin of the t(8;16)(p11;p13). Genes Chromosomes Cancer 2003;36:90–8.
49. Panagopoulos I, Fioretos T, Isaksson M, et al. RT-PCR analysis of acute myeloid leukemia with t(8;16)(p11;p13): identification of a novel MOZ/CBP transcript and absence of CBP/MOZ expression. Genes Chromosomes Cancer 2002;35:372–4.
50. Panagopoulos I, Isaksson M, Lindvall C, et al. RT-PCR analysis of the MOZ-CBP and CBP-MOZ chimeric transcripts in acute myeloid leukemias with t(8;16)(p11; p13). Genes Chromosomes Cancer 2000;28:415–24.